



RESEARCH ARTICLE

Design of a wire-driven parallel robot for wind tunnel test based on the analysis of stiffness and workspace

Yangfeng Ji¹ , Miaojiao Peng²  and Qi Lin³

¹Chengyi College, Jimei University, Xiamen, Fujian, PR China

²School of Marine Engineering, Jimei University, Xiamen, Fujian, PR China

³Department of Aircraft, Xiamen University, Xiamen, Fujian, PR China

Corresponding authors: Miaojiao Peng; Email: pmj1819@163.com; Qi Lin; Email: qilin@xmu.edu.cn

Received: 22 March 2024; **Revised:** 26 June 2024; **Accepted:** 9 August 2024; **First published online:** 5 November 2024

Keywords: wind tunnel test; wire-driven parallel robot; stiffness analysis; wire tension; suspension scheme design

Abstract

This paper presents an eight wire-driven parallel robot (WDPR-8) designed to serve as a suspension manipulator for aircraft models during wind tunnel testing. The precision of these tests is significantly influenced by the system's stability and workspace, both of which are shaped by the geometric configuration of the structure and the tension in the wires. To acquire the efficiency principle of the suspension scheme design for the model, a kinematics model for a WDPR-8 was established. Based on the kinematics model, the stiffness of a WDPR-8 was theoretically studied, and the analytical expression of stiffness matrix of a WDPR was deduced. The stiffness matrix was composed of two terms, one of which is determined by the configuration of suspension system and the other term is determined by the wire tension. Based on the analysis result, a set of suspension scheme was discussed under the calculation of stiffness matrix and workspace analysis. In the discussion process, in addition to the stiffness-maximum calculation, another criterion as force closure is presented, which is useful for increasing the stiffness and workspace of the robot. Finally, a prototype was established according to the analysis result, and the workspace experiments are conducted. Test results indicate that the workspace meets the design requirements, validating the system suspension design method of a WDPR for aircraft model suspension in wind tunnel test considering of the systematic stiffness and workspace.

Nomenclature

B_i	hinge point on the robot base
f_G	gravity force
J_A	Jacobian matrix of WDPR
K	stiffness vector of system
L	wire vector L_i
\tilde{L}	diagonal matrix of L_i
L_i	length of i th wire
$O_g x_g y_g z_g$	global coordinate system
$O_b x_b y_b z_b$	body coordinate system
P	barycenter of the aircraft model
P_i	anchor point on the aircraft model
V	airspeed in wind tunnel, m/s
r	vector in body coordinate system

\mathbf{R}	transformation matrix
\mathbf{R}°	spinor symmetric matrix of \mathbf{R}
\mathbf{u}_i	unit vector of wire
\mathbf{W}_R	wretch vector acting on model
X_P	pose vector of the aircraft model
$\dot{\mathbf{X}}_\omega$	velocity vector of the aircraft model
φ	roll angle, degrees
θ	angle of attack, degrees
ψ	yaw angle, degrees
ω	angle velocity, rad/s

1. Introduction

Wind tunnel testing is an indispensable component in the development of new aerospace vehicles. The model mount is a device that holds a test model in a required position, or controls the position and attitude of the model in the test section of the wind tunnel [1]. Compared with conventional rigid-link support systems, a wire-driven parallel robot (WDPR) as a model mount system possesses several merits such as negligible flow field interference [2], larger workspace [3], higher payload-to-weight ratio, and lower manufacturing costs [4]. In addition, they have received significant interest for use in applications such as very-large radio telescope systems [5], rehabilitation [6, 7], and material painting [8].

The use of WDPRs in wind tunnel testing is a burgeoning application. Technical issues of this kind of WDPRs, such as kinematics [9], singularity [10, 11], workspace determination [12–14], cable tensions distribution [15], trajectory control [16, 17], and redundancy [18], have been widely investigated. Given the unidirectional nature of cable tension, maintaining positive tension in all wires is essential for effective load transmission. As a result, the wire tension and the configuration of the support system have perceptible influence on stiffness of the system, which is the key issue for the performance and stability of the suspension system.

The active suspension system for the wind tunnel tests project *Suspension active pour essais en soufflerie*, one representative example of WDPR, is sponsored by Office National d'Etudes et Recherches Aérospatiales and has been utilized in wind tunnel tests in the design of novel fighters [19, 20]. A wire-driven parallel suspension system with eight wires (WDPSS-8) was developed as a mount mechanism and were successfully used in wind tunnel test [21, 22]. In another study by Yue et al. [23], the stiffness of the wire-driven parallel manipulator is theoretically studied, and the results were validated through simulation of the system stiffness matrix. In ref. [24], the stiffness-feasible workspace is introduced based on analyzing in detail the stiffness of the CDPRs. In addition, a planar cable robot is optimally designed with the stiffness-feasible workspace as the performance index. Han Yuan and Eric Courteille et al. [25] analyzed the dynamic and static stiffness of the CDPRs with a non-negligible cable elasticity and mass. In a study by Xiong et al. [26], the influence of the wire tensions on the CDPRs' stiffness was explored. The simulation results indicated that increasing the antagonistic wire tensions does not increase the CDPRs' stiffness within a certain set of poses. In another investigation by Xiong et al. [27], the influence of the specific stiffness and cable strain on the CDPR stiffness was examined. This led to the proposal of the concept of the stiffness change ratio to reflect how significantly the stiffness can be regulated at a specific pose. Ferravante [28] proposed a modeling strategy for cable-driven parallel robots, in which the finite element method was used for cables modeling in order to account for their mass and stress-dependent stiffness and the relevant dynamics was neglected. Mousavi MR et al. [29] investigated a noniterative analytical approach to plan the safe wire tension distribution along with the cables in the redundant cable-driven parallel robots. The proposed algorithm considers not only tracking the desired trajectory but also protecting the system against possible failures. Yu et al. [30] established the stiffness model of CDPR. The stability factor was proposed to evaluate the stability of the robot and

a stability feasible workspace (SFW) based on the stability requirements of the CDPR and an algorithm based on convex set theory to create the SFW are developed.

Previous research has often overlooked the interplay between a WDPR's stiffness and tension in the design phase, particularly because these robots were not commonly applied to wind tunnel testing. As a result, although WDPRs were used as a model mount in the last decades, one cannot see clearly how efficiently a WDPR is established. By taking into account the system's stiffness in the construction of prototype, this study aims to develop a succinct suspension design method of a WDPR. Thus, one can intuitively understand how the geometric structure and the specific wire tension contribute to the stiffness of the WDPR, which is meaningful for the application of the WDPR as a model suspension system in wind tunnel test.

This paper details an efficiency wire-driven parallel suspension system design strategy for wind tunnel test application with the consideration of system stiffness and wire tension. This investigation is based on a previous research [23]. Compared to literature [23], innovative work in this article includes the mathematically decoupled stiffness model of a general WDPR and the prototype construction method with the consideration of systematic stiffness and system workspace.

This work is structured as follows. Section II provides a detailed description of the supporting mechanism of the WDPR with eight wires (WDPR-8) used in this work. In section III, the suspension scheme and the kinematic relationship analysis of WDPR-8 are established. The development of a mathematical expression stiffness matrix of a WDPR is presented. Section IV presents the force-closure condition for the calculation of stiffness during the following work. In section V, the standard dynamic model (SDM) as suspension model is presented. Four different suspension schemes were constructed under the same wire tension condition, and the stiffness matrix of the suspension manipulator were calculated, and the results were deeply discussed. In section VI, A prototype was established according to the analysis result, and the workspace experiments were conducted. The test data were analyzed, and the result was discussed, validating the system suspension design method with the consideration of the systematic stiffness and wire tension. Finally, the main results of this work were summarized, and some conclusions were delivered in section VII.

2. Description of WDPR-8

A simplified structure of a typical WDPR-8 in this work is illustrated in Figure 1(a), in which a fuselage is suspended in the middle of the framework. Figure 1(b) shows a partial enlarged view of the aircraft model in Figure 1(a) and displays the wire joint points on the model more clearly.

Considering the symmetry of the aircraft model, 8 wires are used to support the model in this manuscript, as shown in Figure 1(b). One end of each wire is attached, respectively, to P_i ($i = 1, 2, \dots, 8$) on the aircraft model, and the other end is connected, respectively, to a slider on the ball screw through a universal pulley B_i ($i = 1, 2, \dots, 8$) fixed on the frame. When the length of the eight suspension wires change, the aircraft model rotates around the axis or translates along the axis.

For the convenience of further analysis, a global coordinate system $O_g x_g y_g z_g$ and a body coordinate system $O_b x_b y_b z_b$ were set up, as shown in Figure 1(a). In the body coordinate system $O_b x_b y_b z_b$, the origin is set at the barycenter P of the model. The $O_b x_b$ axis coincides with the axis of the fuselage and is directed toward the nose of the model. The $O_b y_b$ axis points toward the right wing tip. Finally, the $O_b z_b$ axis is determined in accordance with the right-hand rule and is perpendicular to the other two axes. The three coordinates of $O_g x_g y_g z_g$ are in the same direction as the three corresponding coordinates of $O_b x_b y_b z_b$, and the origin point O_g is directly below O_b .

3. Stiffness analysis strategy

The kinematic relationship of WDPR-8 is illustrated in Figure 2. For the convenience of expression, the aircraft model is simplified as a bold cross. Its long axis coincides with the main axis of the model

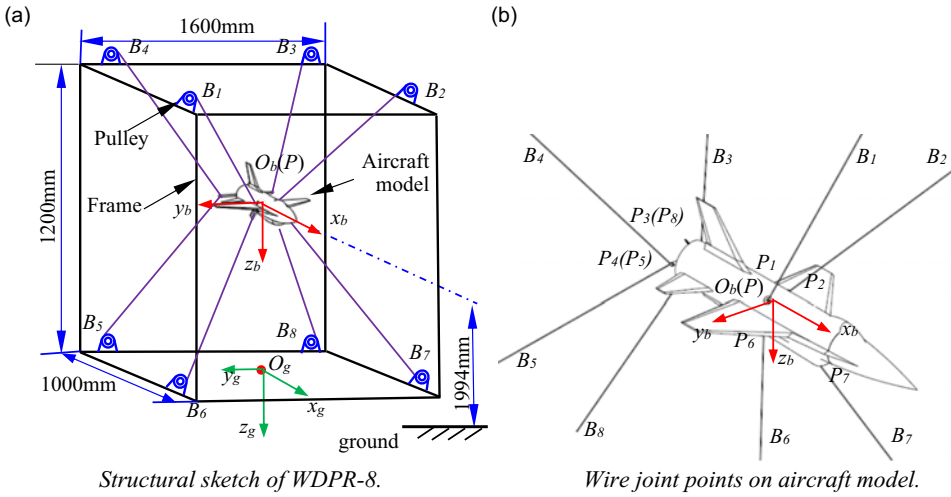


Figure 1. Schematic structure of WDPR-8.

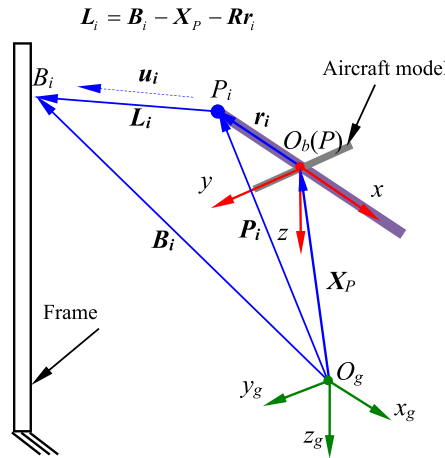


Figure 2. Illustration of the kinematic relationship in WDPR-8.

fuselage, and the lateral axis is parallel to the direction of the model wingspan. In Figure 2, the vector $r_i = \overrightarrow{O_b P_i}$ is defined in body coordinate system $O_b x_b y_b z_b$, and the vectors $B_i = \overrightarrow{O_g B_i}$, $X_p = \overrightarrow{O_g O_b}$, $P_i = \overrightarrow{O_g P_i}$, $u_i = \overrightarrow{P_i B_i}$ are defined in the global coordinate system $O_g x_g y_g z_g$. In global coordinate, the wire vector L_i is defined as

$$L_i = B_i - X_p - R r_i \tag{1}$$

where $X_p(X, Y, Z)^T$ is the coordinate position of the coordinate origin of body coordinate $O_b x_b y_b z_b$ in the global coordinate $O_g x_g y_g z_g$; R is the transition matrix from body coordinate to global coordinate

$$R = \begin{bmatrix} c\theta c\psi & s\phi s\theta c\psi - c\phi s\psi & c\phi s\theta c\psi + s\phi s\psi \\ c\theta s\psi & s\phi s\theta s\psi + c\phi c\psi & c\phi s\theta s\psi - s\phi c\psi \\ -s\theta & s\phi c\theta & c\phi c\theta \end{bmatrix} \tag{2}$$

where c and s is short for \cos and \sin , and ϕ, θ, ψ is the angular displacement of the aircraft model around $O_g x_g$ -axis, $O_g y_g$ -axis, and $O_g z_g$ -axis, respectively.

Let $\mathbf{X} = (X_p, Y_p, Z_p, \varphi, \theta, \psi)^T$ be the pose vector of the aircraft model, and $\dot{\mathbf{X}}_\omega = (\dot{X}_p, \dot{Y}_p, \dot{Z}_p, \omega_x, \omega_y, \omega_z)^T$ be the velocity vector. According to differential kinematics of parallel mechanisms

$$\dot{\mathbf{L}} = \mathbf{J}_A \dot{\mathbf{X}}_\omega \tag{3}$$

where \mathbf{J}_A^T is the Jacobi matrix of WDPR-8. It is defined by the parameters of WDPR-8, the expression of which is

$$\mathbf{J}_A^T = \begin{bmatrix} \mathbf{u}_1 & \cdots & \mathbf{u}_8 \\ \mathbf{r}_1 \times \mathbf{u}_1 & \cdots & \mathbf{r}_8 \times \mathbf{u}_8 \end{bmatrix} \tag{4}$$

The relationship between the pose or velocity of the aircraft model and the wire length L_i ($i = 1, 2, \dots, 8$) is determined according to Eqs. (1)–(4). The change in the three rotational degrees and the three transitional degrees of the model can be transformed to a variation in the supporting wire length.

The length of L_i ($i = 1, 2, \dots, 8$) is obtained through the transformation of (1)

$$L_i^2 = (\mathbf{B}_i - \mathbf{X}_p - \mathbf{R}\mathbf{x}_{pi})^T (\mathbf{B}_i - \mathbf{X}_p - \mathbf{R}\mathbf{x}_{pi}) \tag{5}$$

Differentiate (5) with respect to time

$$2L_i \dot{L}_i = (\dot{\mathbf{X}}_p + \dot{\mathbf{R}}\mathbf{x}_{pi})^T (\mathbf{B}_i - \mathbf{X}_p - \mathbf{R}\mathbf{x}_{pi}) + (\mathbf{B}_i - \mathbf{X}_p - \mathbf{R}\mathbf{x}_{pi})^T (\dot{\mathbf{X}}_p + \dot{\mathbf{R}}\mathbf{x}_{pi}) \tag{6}$$

Formula (6) is simplified as

$$2L_i \dot{L}_i = 2(\mathbf{B}_i - \mathbf{X}_p - \mathbf{R}\mathbf{x}_{pi})^T (\dot{\mathbf{X}}_p + \dot{\mathbf{R}}\mathbf{x}_{pi}) \tag{7}$$

Substituting (1) into (7)

$$L_i \dot{L}_i = (\mathbf{L}_i)^T (\dot{\mathbf{X}}_p + \dot{\mathbf{R}}\mathbf{x}_{pi}) \tag{8}$$

In addition, the derivative of the rotation and transformation matrix \mathbf{R} with respect to time in (2) is

$$\dot{\mathbf{R}} = \mathbf{R}^\circ \mathbf{R} \tag{9}$$

where $\mathbf{R}^\circ = \begin{bmatrix} 0 & -\omega_z & \omega_y \\ \omega_z & 0 & -\omega_x \\ -\omega_y & \omega_x & 0 \end{bmatrix}$ is the spinor symmetric matrix of \mathbf{R} , and $\omega_x, \omega_y, \omega_z$ are the angular velocity of the moving platform around three corresponding coordinate axes.

Substituting (9) into (8), then

$$L_i \dot{L}_i = (\mathbf{L}_i)^T (\dot{\mathbf{X}}_p + \mathbf{R}^\circ \mathbf{R}\mathbf{x}_{pi}) \tag{10}$$

In Figure 2, the vector $\mathbf{r}_i = \mathbf{R}\mathbf{x}_{pi}$, then

$$L_i \dot{L}_i = (\mathbf{L}_i)^T \dot{\mathbf{X}}_p + (\mathbf{L}_i)^T (\boldsymbol{\omega} \times \mathbf{r}_i) \tag{11}$$

Further simplification of (11) is

$$L_i \dot{L}_i = (\mathbf{L}_i)^T \dot{\mathbf{X}}_p + \mathbf{r}_i \times \mathbf{L}_i^T \boldsymbol{\omega} \tag{12}$$

Taking all the eight wires of WDPR-8 into consideration, (12) is expressed in matrix form

$$\tilde{\mathbf{L}} \dot{\mathbf{L}} = \tilde{\mathbf{J}}_A \dot{\mathbf{X}}_\omega \tag{13}$$

The matrices in (13) are defined as

$$\begin{aligned} \tilde{\mathbf{L}} &= \text{diag}[L_1, L_2, \dots, L_8], \dot{\mathbf{L}} = [\dot{L}_1, \dot{L}_2, \dots, \dot{L}_8]^T, \dot{\mathbf{X}}_\omega = \begin{bmatrix} \dot{\mathbf{X}}_p \\ \boldsymbol{\omega} \end{bmatrix} = \begin{bmatrix} v \\ \boldsymbol{\omega} \end{bmatrix}, \\ \tilde{\mathbf{J}}_A^T &= \begin{bmatrix} \mathbf{L}_1 & \mathbf{L}_2 & \cdots & \mathbf{L}_8 \\ \mathbf{r}_1 \times \mathbf{L}_1 & \mathbf{r}_2 \times \mathbf{L}_2 & \cdots & \mathbf{r}_8 \times \mathbf{L}_8 \end{bmatrix}. \end{aligned}$$

where \dot{X}_ω is the velocity vector of the moving platform, including the linear velocity v and angular velocity ω . (13) is left multiplied by \tilde{L}^{-1} on both sides

$$\dot{L} = \tilde{L}^{-1} \tilde{J}_A \dot{X}_\omega = J_A \dot{X}_\omega \tag{14}$$

Eqs. (14) is the relationship between the velocity vector of driving wire and the velocity vector of the aircraft model. (14) is taken the derivative of time, then

$$\ddot{L} = J_A \ddot{X}_\omega + \dot{J}_A \dot{X}_\omega \tag{15}$$

Eqs. (12) can be transformed as

$$\dot{L}_i = u_i^T \dot{X}_p + r_i \times u_i^T \omega \tag{16}$$

where

$$\dot{L}_i = \dot{L}_i u_i + L_i \dot{u}_i = (\dot{X}_p + r_i)' = \dot{X}_p - r_i \times \omega \tag{17}$$

Substituting (16) into (17)

$$\dot{u}_i = \frac{1}{L_i} [(I - u_i u_i^T) \dot{X}_p - (I - u_i u_i^T) r_i \times \omega] \tag{18}$$

Through the above derivation, it can be concluded that

$$J_A^T = [J_{A1} \ J_{A2} \ J_{A3} \ J_{A4} \ J_{A5} \ J_{A6} \ J_{A7} \ J_{A8}] \tag{19}$$

where the expression for any components of (19) is

$$J_{Ai}^T = \begin{bmatrix} \frac{1}{L_i} [(I - u_i u_i^T) \dot{X}_p - (I - u_i u_i^T) r_i \times \omega] \\ (\omega \times r_i) \times u_i + r_i \times \frac{1}{L_i} [(I - u_i u_i^T) \dot{X}_p - (I - u_i u_i^T) r_i \times \omega] \end{bmatrix} \tag{20}$$

In WDPR-8, the wire tension matrix $T = (T_1, T_2, T_3, T_4, T_5, T_6, T_7, T_8)^T$ and the external forces and wrench vectors W_R acting on the model are unified in the formula

$$W_R = J_A^T T \tag{21a}$$

Giving a slight variation ∂W_R to W_R , a corresponding slight variation ∂X will occur in the pose $X = (X_p, Y_p, Z_p, \varphi, \theta, \psi)^T$ of the aircraft model. ∂X is defined as $\partial X = [\partial x^T, \partial \mu^T]^T$, where $\partial x = [\varepsilon_x, \varepsilon_y, \varepsilon_z]^T$ is the differential displacement and $\partial \mu = [\mu_x, \mu_y, \mu_z]^T$ is the differential rotation. According to the basic principle of differential transformation, the static stiffness of WDPR is defined as

$$\partial W_R = K \partial X \tag{21b}$$

Taking variation at both sides of (21a), then

$$\partial W_R = \partial J_A^T T + J_A^T \partial T \tag{22}$$

Taking the derivative of Jacobi matrix

$$J_A^T = \begin{bmatrix} \dot{u}_1 & \dot{u}_2 & \cdots & \dot{u}_8 \\ (\omega \times r_1) \times u_1 + r_1 \times \dot{u}_1 & (\omega \times r_2) \times u_2 + r_2 \times \dot{u}_2 & \cdots & (\omega \times r_8) \times u_8 + r_8 \times \dot{u}_8 \end{bmatrix} \tag{23}$$

Assuming that the endpoint P_i of the moving platform generates a slight motion vector, the derivative of wire i direction vector can be expressed as

$$\begin{aligned} \dot{u}_i &= \frac{1}{L_i} \{ (I_3 - u_i u_i^T) \dot{X}_p - (I_3 - u_i u_i^T) r_i \times \omega \} \\ &= \frac{1}{L_i} [(I_3 - u_i u_i^T) - (I_3 - u_i u_i^T) r_i \times] D \dot{X} \end{aligned} \tag{24}$$

where $\mathbf{r}_i \times = \begin{bmatrix} 0 & -r_z & r_y \\ r_z & 0 & -r_x \\ -r_y & r_x & 0 \end{bmatrix}$ is the spinor symmetric matrix, and \mathbf{I}_3 is the 3rd order unit matrix.

Right crossing \mathbf{u}_i to both sides of (17)

$$(\boldsymbol{\omega} \times \mathbf{r}_i) \times \mathbf{u}_i = (\mathbf{L}_i \dot{\mathbf{u}}_i - [\mathbf{I}_3 \quad \mathbf{0}] \dot{\mathbf{X}}) \times \mathbf{u}_i \tag{25}$$

Where $[\mathbf{I}_3 \quad \mathbf{0}]$ is the 3×6 partitioned matrices and $\mathbf{0}$ is three-dimensional zero matrix.

Substituting (25) into (24), then each term of (23) is expressed as

$$\begin{bmatrix} \dot{\mathbf{u}}_i \\ (\boldsymbol{\omega} \times \mathbf{r}_i) \times \mathbf{u}_i + \mathbf{r}_i \times \dot{\mathbf{u}}_i \end{bmatrix} = \begin{bmatrix} \mathbf{U}_i \dot{\mathbf{X}} \\ -\mathbf{u}_i \times (\mathbf{L}_i \mathbf{U}_i - [\mathbf{I}_3 \quad \mathbf{0}]) \dot{\mathbf{X}} + \mathbf{r}_i \times \mathbf{U}_i \dot{\mathbf{X}} \end{bmatrix} \tag{26}$$

where $\mathbf{U}_i = \frac{1}{L_i} [(\mathbf{I}_3 - \mathbf{u}_i \mathbf{u}_i^T) - (\mathbf{I}_3 - \mathbf{u}_i \mathbf{u}_i^T) \mathbf{r}_i \times] \mathbf{D}$.

Combining (23) and (26), then

$$\partial \mathbf{J}_A^T \mathbf{T} = \sum_{i=1}^8 \begin{bmatrix} \mathbf{U}_i \\ -\mathbf{u}_i \times (\mathbf{L}_i \mathbf{U}_i - [\mathbf{I}_3 \quad \mathbf{0}]) + \mathbf{r}_i \times \mathbf{U}_i \end{bmatrix} T_i \partial \mathbf{X} \tag{27}$$

If external forces are acted on the aircraft model, a micro variable $\partial \mathbf{L}$ will generates in the wire length vector $\mathbf{L} = [L_1 \ L_2 \ \dots \ L_8]^T$. Based on the principle of virtual work, the relationship between $\partial \mathbf{L}$ and $\partial \mathbf{X}$ will be

$$\mathbf{T}^T \partial \mathbf{L} = \mathbf{W}_R^T \partial \mathbf{X} \tag{28}$$

Substituting $\mathbf{W}_R = \mathbf{J}_A^T \mathbf{T}$ into (28)

$$\partial \mathbf{L} = \mathbf{J}_A \partial \mathbf{X} \tag{29}$$

Using \mathbf{K}_m to represent the stiffness matrix of the support wires, the slight wire length variable $\partial \mathbf{L}$ and the corresponding micro variable of wire tension $\partial \mathbf{T}$ satisfies

$$\partial \mathbf{T} = \mathbf{K}_m \partial \mathbf{L} \tag{30}$$

Substituting (29) and (30) into the second term of (22)

$$\mathbf{J}_A^T \partial \mathbf{T} = \mathbf{J}_A^T \mathbf{K}_m \mathbf{J}_A \partial \mathbf{X} = \mathbf{J}_A^T \text{diag}(\mathbf{v}) \mathbf{J}_A \partial \mathbf{X} \tag{31}$$

where $\mathbf{v} = [\frac{k}{L_1} \ \frac{k}{L_2} \ \dots \ \frac{k}{L_8}]$. k is the unit stiffness of wire and L_i is the length of i th wire.

Substituting (27) and (31) into (22), and combining the result with (21b), the stiffness of WDPR-8 is formulated as

$$\mathbf{K} = \sum_{i=1}^8 \begin{bmatrix} \mathbf{U}_i \\ -\mathbf{u}_i \times (\mathbf{L}_i \mathbf{U}_i - [\mathbf{I}_3 \quad \mathbf{0}]) + \mathbf{r}_i \times \mathbf{U}_i \end{bmatrix} T_i + \mathbf{J}_A^T \text{diag}(\mathbf{v}) \mathbf{J}_A \tag{32}$$

Eqs. (32) indicates that the stiffness of WDPR-8 is composed of the follow two parts

$$\begin{cases} \mathbf{K}_1 = \sum_{i=1}^8 \begin{bmatrix} \mathbf{U}_i \\ -\mathbf{u}_i \times (\mathbf{L}_i \mathbf{U}_i - [\mathbf{I}_3 \quad \mathbf{0}]) + \mathbf{r}_i \times \mathbf{U}_i \end{bmatrix} T_i \\ \mathbf{K}_2 = \mathbf{J}_A^T \text{diag}(\mathbf{v}) \mathbf{J}_A \end{cases} \tag{33}$$

where \mathbf{K}_1 is determined by the wire tension and \mathbf{K}_2 is the characteristic parameters of WDPR, which is determined by the geometric arrangement of wires and the position of universal pulleys on the braced frame, as shown in Figure 1(a).

4. Tension solution under the force-closure condition

Force-closure analysis is a commonly employed workspace analysis tool for fully-constrained WDPR [31, 32]. The mathematical description for the force-closure condition is $\mathbf{W}_R = \mathbf{J}_A^T \mathbf{T}$, where $\mathbf{W}_R = [\mathbf{f}_G \quad \mathbf{0}]^T$ is the external wrench exerted on the aircraft model.

The necessary conditions to attain force closure are

- (1) The tension in each wire can always be made positive regardless of the external wrench.
- (2) All the wire tension varies between a fixed interval $[T_{\min}, T_{\max}]$:

$$0 < T_{\min} \leq T_i \leq T_{\max}, i \in [1, 8] \tag{33}$$

According to the Van Hough’s theory, in order to find continuous solution for wire tension, the above conditions can be equivalently transformed into a P-norm optimization problem

$$\begin{cases} f(T)_{\min} = \|T\|_p = \sqrt{\sum_{i=1}^m T_i^2} \\ T_{\min} \leq T_i \leq T_{\max} \\ W_i = -\sum_{j=1}^m J_{A_i}^T, T_i \end{cases} \tag{34}$$

For any wire tension T_i

$$T = T_A + T_R \tag{35}$$

where $T_A = (T_{\min} + T_{\max})/2$, and T_R is a arbitrary vector.

Substituting (35) into (22):

$$J_A^T T_R = W_R - J_A^T T_A \tag{36}$$

Let J_A^{T+} be the pseudo-inverse matrix of J_A^T

$$J_A^{T+} = J_A (J_A^T J_A)^- \tag{37}$$

Both sides of (36) are multiplied by J_A^{T+} from the left

$$T_R = J_A^{T+} (W_R - J_A^T T_A) \tag{38}$$

Substituting (38) back into (35), then the wire tension is

$$T = T_A + J_A^{T+} (W_R - J_A^T T_A) \tag{39}$$

Substituting (39) into (33), the stiffness of a WDPR will be determined.

5. Design and improvement of WDPR-8 suspension scheme

5.1. Suspension model

The SDM, first introduced by National Aeronautical Establishment (NAE) [33, 34], was adopted as the suspension model in this paper. The SDM in this manuscript is 0.36 times the size of the original model of NAE. The maximum length, the fuselage diameter, and the wingspan of the model were 378 mm, 54 mm, and 244 mm, and the mass is 1.093 kg, as shown in Figure 3 and Table I.

The SDM used in this article, which evolved from the F16, retains the basic external characteristics of a fighter including slender fuselage, thin wings, and widely distributed strake wings, making it impossible to arrange wire joint points at the wing tips, fuselage sides, or even nose. According to the characteristics of the complete symmetry between the left and right sides of the fuselage, the arrangement of the suspension wires should be as symmetrical as possible. As shown in Figure 1(b), the four wires in front were attached to four struts evenly around the aircraft model, the extension lines of four struts converge along radial to the point P on the model, which is also the barycenter of the model. The four wires at the tail of the aircraft were tied to the two ends of a horizontal bar connected to the fuselage.

Table I. Detailed parameters of SDM.

Parameter	Value
Mass	1.093 kg
Inertia	
I_{xx}	$6.84 \times 10^{-4} \text{ kgm}^2$
I_{yy}	$8.52 \times 10^{-3} \text{ kgm}^2$
I_{zz}	$8.46 \times 10^{-3} \text{ kgm}^2$
Wing reference area	$1.99 \times 10^{-2} \text{ m}^2$
Mean aerodynamic chord	0.092 m

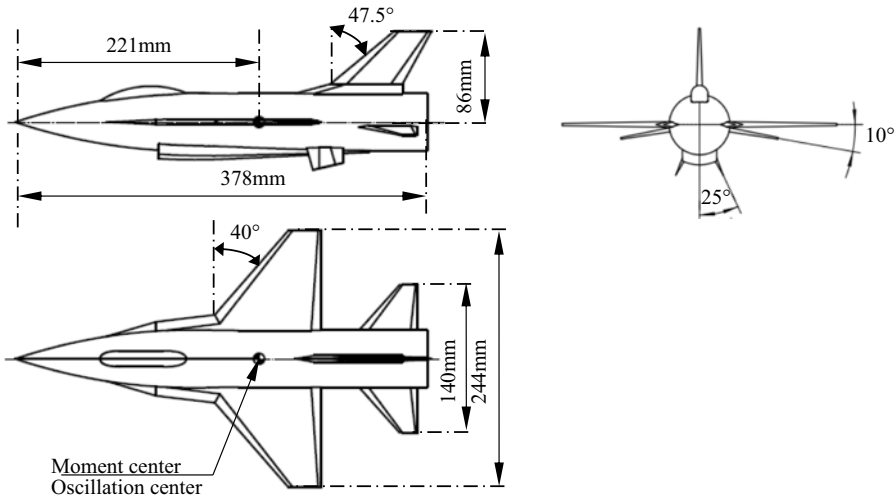


Figure 3. Standard dynamic model (SDM).

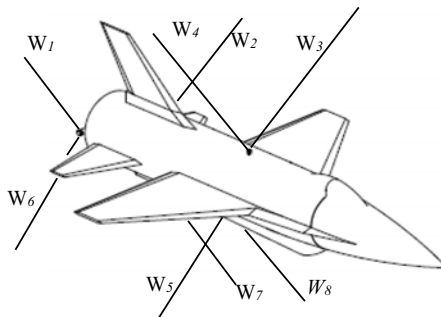


Figure 4. Suspension scheme 1 for WDPR-8.

5.2. Design and improvement of suspension scheme for WDPR-8

5.2.1. Suspension scheme 1

Figure 4 is the original suspension scheme, while $W_i (i = 1 \dots 8)$ represents the eight suspension wires. The hinge points $P_i (i = 1, 2, \dots, 8)$ on the aircraft model and the universal pulleys $B_i (i = 1, 2, \dots, 8)$ on the prototype are shown in Table II. The position between the origin point O_g and the original point O_b is decided by the vector $X_p = (0, 0, -582)^T$.

Table II. The hinge points P_i and B_i of scheme 1.

i	P_i			B_i		
	x_b	y_b	z_b	x_g	y_g	z_g
1	0	0	-27	472	815	-1286
2	0	0	27	515	-772	-1286
3	-165	-24	0	-472	-815	-1286
4	-165	24	0	-515	772	-1286
5	-165	24	0	-472	815	-71
6	0	0	33	515	772	-71
7	0	0	33	472	-815	-71
8	-165	-24	0	-515	-772	-71

As can be seen in Figure 4, the front wires W_3 and W_4 (W_5 and W_8) were attached to the same hinge point, respectively, whereas the four rear wires W_1 and W_6 (W_2 and W_7) were attached to two ends of a horizontal bar fixed two the aircraft model.

The obvious advantages of suspension scheme 1 are the minimum influence to the fuselage.

Assuming that the wire tension $T_{\min} = [20, 20, 20, 20, 20, 20, 20, 20]^T$ and $T_{\max} = [50, 50, 50, 50, 50, 50, 50, 50]^T$. According to the force-closure condition, the tension of eight wires was calculated, and the system stiffness matrix of WDPR-8 is calculated according to equation (32)

$$K = \begin{bmatrix} 9704 & 373 & -516 & 120 & 305 & -17 \\ 373 & 35294 & -173 & -356 & -105 & -2925 \\ -516 & -173 & 20260 & -180 & 1960 & -15 \\ 120 & -363 & -182 & 21 & 0 & 10 \\ 305 & -105 & 1960 & 0 & 310 & -3 \\ -17 & -2925 & -15 & 2 & -3 & 446 \end{bmatrix}$$

The six values on the main diagonal in the stiffness matrix represent the three translation stiffness (N/m) along $O_g x_g, O_g y_g, O_g z_g$ and three rotational stiffness (N · m/rad) around the three axis, respectively, and the rest values in the matrix are the coupling stiffness. For the convenience of discussion in the rest of this work, the six values on the main diagonal are selected to form a diagonal matrix

$$diag(K)_1 = [9704, 35294, 20260, 21, 310, 446]^T \tag{40}$$

The final three values in the matrix correspond to the roll, pitch, and yaw stiffness. Notably, the roll stiffness is significantly lower than the other two, leading to instability during roll testing. The reason of this phenomenon is that W_3 and W_4 are attached to the same point. From the unilateral tension characteristic of the wires, it is not difficult to find out that when the model rotates around $O_g x_g$ axis, tension of wire 3 and wire 8 will increase, and the tension of wire 4 and wire 5 will decrease, causing a decrease in roll stiffness.

5.2.2. Suspension scheme 2

An improvement to suspension scheme 1 was made to testify the analysis above. The detailed parameters of P_i and B_i are shown in Table III. The four rear wires ($W_1, W_6, W_2,$ and W_7) are the same as scheme 1, and the front four wires were evenly attached to the fuselage, as shown in Figure 5.

T_{\min} and T_{\max} are assigned the same value as in suspension scheme 1, and the diagonal stiffness matrix $diag(K)_2$ of WDPR-8 in Figure 5 is calculated according to (32)

$$diag(K)_2 = [9626, 35534, 21582, 28, 323, 368]^T \tag{41}$$

Table III. The hinge points P_i and B_i of scheme 2.

i	P_i			B_i		
	x_b	y_b	z_b	x_g	y_g	z_g
1	30	19	-19	472	515	-1286
2	30	-19	-19	515	-515	-1286
3	-165	-53	0	-472	-515	-1286
4	-165	53	0	-515	515	-1286
5	-165	53	0	-472	515	-71
6	30	19	19	515	515	-71
7	30	-19	19	472	-515	-71
8	-165	-53	0	-515	-515	-71

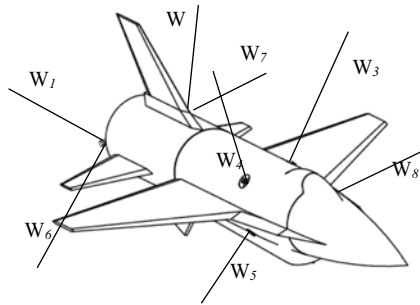


Figure 5. Suspension scheme 2 for WDPR-8.

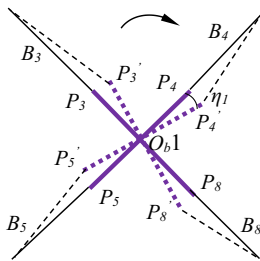


Figure 6. Front view of suspension scheme 2.

The result of suspension scheme 2 shows the slight increase of roll stiffness. The front view and the rear view of the suspension wires are shown in Figure 6 and Figure 7, respectively. The thick purple cross in Figure 6 represents the aircraft model, and the thick purple line in Figure 7 denotes a horizontal metal rod fixed to the aircraft model. The solid lines indicate the original position of the wires, and the dashed lines represent the new position of the wires when the aircraft model rotates a slight angle η_1 (φ_1).

Taking wire B_3P_3 as an example, a reverse torque will act on the model by B_3P_3' while the model rotates slight angle η_1 to reach the dashed line position, as shown in Figure 6, resulting a decrease in the roll stiffness because of the unilateral characteristics of the wires. Similar situations also occur in the four rear wires in Figure 7. When the model rotates a slight angle φ_1 to the dotted line position, reverse torques will in the four wires and decrease the roll stiffness.

Further analysis shows that the rear four wires provide more torque to change the angle of the model, because the attach point P_1 and P_6 (P_2 and P_7) will provide longer force arms compared with P_3 and P_4 (P_5 and P_8), as shown in Figure 6 and Figure 7. When the roll angle φ_1 is greater than φ_2 , positive torque

Table IV. The hinge points P_i and B_i of scheme 3.

i	P_i			B_i		
	x_b	y_b	z_b	x_g	y_g	z_g
1	0	25	9	472	234	-1286
2	0	-25	9	515	-234	-1286
3	-165	-53	0	-472	-515	-1286
4	-165	53	0	-515	515	-1286
5	-165	53	0	-472	515	-71
6	0	25	-9	515	234	-71
7	0	-25	-9	472	-234	-71
8	-165	-53	0	-515	-515	-71

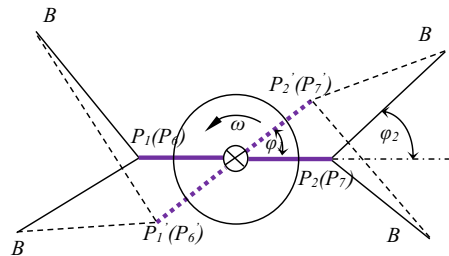


Figure 7. Rear view of suspension scheme 2.

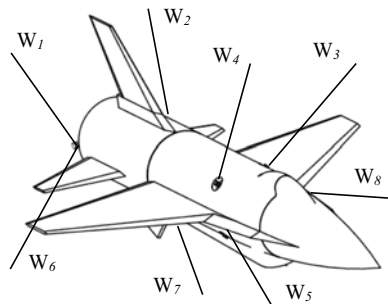


Figure 8. Suspension scheme 3 for WDPR-8.

cannot be provided by the four rear wires for the unilateral tension characteristic of the wires. Thus, the possible improvement direction to raise the roll stiffness is to increase the angle ϕ_2 between the traction rope and the horizontal support rod, as shown in Figure 7.

5.2.3. Suspension scheme 3

Suspension scheme 3 and the corresponding hinge points are designed based on the analysis above as shown in Figure 8 and Table IV. The joint points on the aircraft model (P_i) are the same as in scheme 2, while the hinge points (B_i) on the frame are different.

Substituting the parameters in Table III into (32), the diagonal stiffness matrix of suspension scheme 3 is calculated

$$diag(K)_3 = [23693, 16924, 44922, 83, 597, 256] \tag{42}$$

However increased obviously, calculation result indicates that the roll stiffness was still smaller than pitch and yaw stiffness, so did the pitch workspace. Top view of the suspension was shown in Figure 9

Table V. The hinge points P_i and B_i of scheme 4.

i	P_i			B_i		
	x_b	y_b	z_b	x_g	y_g	z_g
1	0	25	9	472	234	-1286
2	0	-25	9	515	-234	-1286
3	-165	-53	0	-472	-515	-1286
4	-165	53	0	-515	515	-1286
5	-165	53	0	-472	515	-71
6	0	25	-9	515	234	-71
7	0	-25	-9	472	-234	-71
8	-165	-53	0	-515	-515	-71

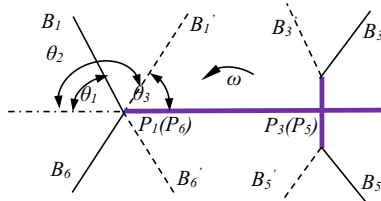


Figure 9. Schematic of pitch workspace for suspension scheme 3.

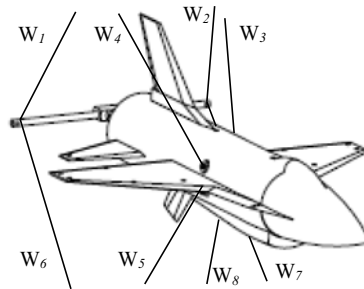


Figure 10. Suspension scheme 4 for WDPR-8.

for further analysis, where the long purple line is the fuselage and the short purple line is the horizontal rod fixed on the fuselage.

5.2.4. Suspension scheme 4

As mentioned above, the rear four wires provide more torque to change the angle of the model. If the model is suspended in the form of the dashed line (wire $P_1 B_1' - P_6 B_6'$ and wire $P_3 B_3' - P_5 B_5'$), the pitch angle θ_1 will approach to θ_2 , which means that the pitch workspace will be greater than 90 degrees. Suspension scheme 4 was designed based on this assumption, as shown in Figure 10, and the corresponding hinge points are shown in Table V. The suspension wires were arranged in symmetrical diamond shape.

According to Table V, the diagonal matrix of stiffness for scheme 4 is

$$diag(K)_4 = [20388, 16255, 56493, 163, 1073, 734]' \tag{43}$$

The roll stiffness increased significantly, and the stability of the platform was simultaneously improved, indicating the feasibility of the improvement direction discussed above. At the same time, the workspace in pitch direction exceeds 60° according to the analysis in Figure 9.

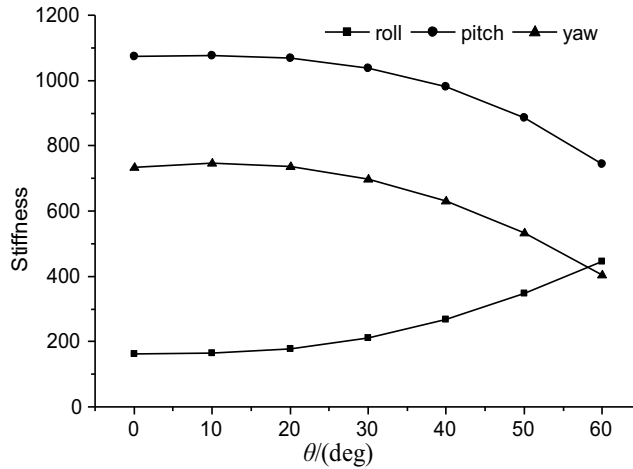


Figure 11. Stiffness of WDPR-8 under different angle of attack.

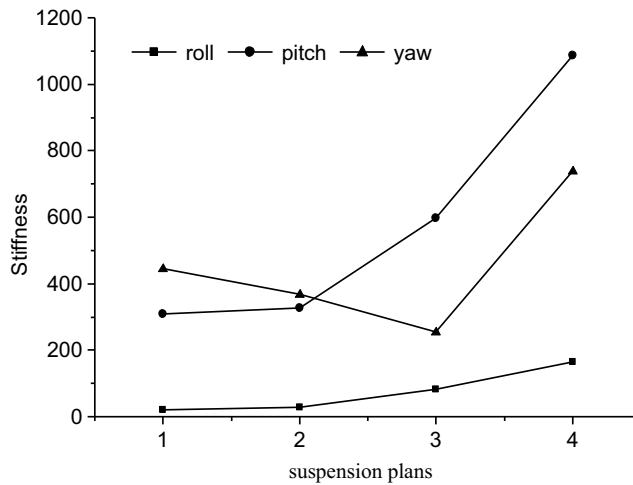


Figure 12. Comparison of rotational stiffness for different suspension schemes.

5.2.5. Further discussion

The above analysis process was conducted at an angle of attack at 0°. The rotational stiffness in roll, pitch, and yaw direction under different angle of attack was calculated, and the results are shown in Figure 11. As illustrated in Figure 11, along with the angle of attack increases, the roll stiffness ascends, while the pitch and yaw stiffness descends slowly. However, the other stiffness is still greater than the roll stiffness when the angle of attack is under about 57°, and the overall stability of the system is guaranteed.

The comparison of stiffness under different suspension schemes discussed in previous chapter is in Figure 12. As depicted in Figure 12, the roll stiffness and pitch stiffness of the system gradually increase, while the yaw stiffness begins to decrease, and all the stiffness was significantly promoted in suspension scheme 4, improving stability of the WDPR as a suspension system in wind tunnel test, and validating the manipulator design method in this work, at least for the standard dynamic model in this paper. Besides, the wires were arranged symmetrically around the aircraft model. However, the wires that determine the yaw workspace are different from that of the workspace in other two direction. As a result, the variation trend of yaw stiffness is different from the trend of other two stiffness.

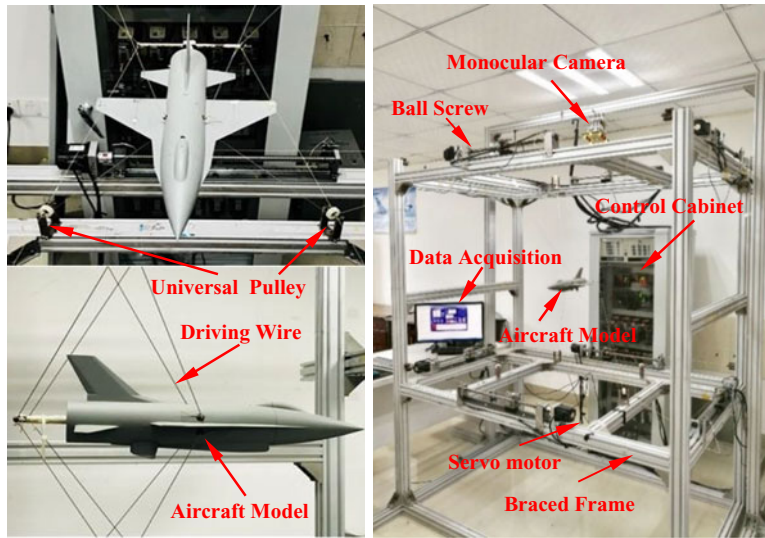


Figure 13. W DPR-8 prototype for experiment.

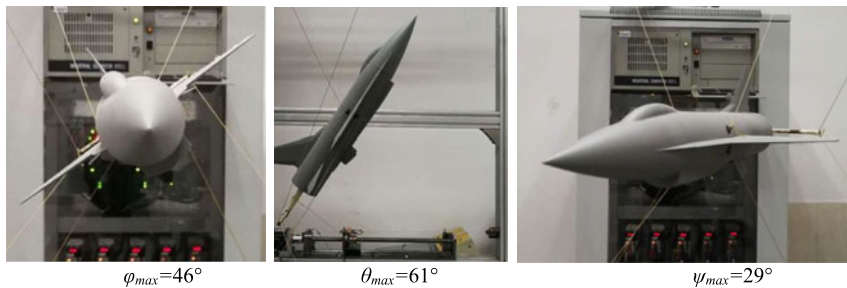


Figure 14. Workspace test of suspension scheme 4.

6. Experiment validation

In order to verify the analysis result of the four suspension scheme, a prototype of W DPR-8 was established for experiments, as shown in Figure 13. The prototype consists of braced frame, eight universal pulleys, eight wires, servo motors, ball screw assemblies, a control cabinet, a aircraft model, as well as a vision measurement system which uses a monocular camera to capture the real-time pose of aircraft model. The aircraft model was suspended in the form of suspension scheme 4, as shown in Figure 10 and the parameters in Table V. The diving wires were arranged in a diamond shape as discussed in suspension scheme 4.

The brace frame of the prototype was constructed using aluminum alloy (No. 6060). In Figure 13, there are eight driving components mounted on the eight horizontal bars of the frame, each of which consists of a ball screw assembly, a servomotor, a driving wire, and a universal pulley. The slider on each ball screw assembly moves back and forth, driven by corresponding motors. Cables with excellent tensile strength and a diameter of 0.5 mm were chosen as the driving wires of the prototype. One end of a wire is attached to a joint point on the aircraft model, and the other end is connected to a slider through the universal pulley. The SDM model was suspended in the middle of the prototype using eight driving wires.

The length of eight wires was changed through the eight servo motors to control the attitude of the aircraft model. When the aircraft model rotates around $O_b x_b$, $O_b y_b$, and $O_b z_b$ axis, the roll angle φ , pitch

angle θ , and yaw angle ψ were recorded while interference was about to occur between the model and wires, so as to obtain the workspace of the institution, as is shown in Figure 14.

Figure 14 shows the experimental results of workspace for suspension scheme 4. The experiments confirmed that the workspace in the pitch direction exceeds 60° , corroborating our analytical predictions, validating the analysis results in Figure 9 and the suspension design methods with the consideration of systematic stiffness and workspace.

7. Conclusions

In this study, an eight WDPR was used as an example to analyze the stiffness of the robot, and the stiffness expression determined by both the wire tension and the geometric structure of the suspension system was deduced. In addition, the suspension wire layouts of the robots with four different configurations were discussed in terms of the diagonal stiffness matrix analysis and, finally, a prototype of a WDPR-8 was established based on the analysis result. The workspace experiments were conducted, the test result was analyzed, and the following conclusions were drawn.

(1) In addition to workspace requirements, the stiffness of the system should be taken into consideration during the design procedure of a WDPR suspension system to improve the stability of the system.

(2) It is not suitable to place connecting points on the wings due to the fact that most aircraft models have thin wings. The suspension wires should be arranged as far away from the fuselage as possible to enhance the system stiffness. For models with symmetrical shapes, it is optimal to adopt a spatial symmetrical layout for the suspension wires.

(3) This research underscores the importance of considering both workspace requirements and system stiffness in the design of WDPR suspension systems. The optimal arrangement of suspension wires, particularly the diamond-shaped symmetrical layout, offers a large workspace and enhanced stiffness, making it a viable option for wind tunnel applications.

While the design requirements outlined here are specific to the SDM support scheme discussed in this paper, they can be broadly applied to the development of wind tunnel suspension systems for a range of models. The design procedure based on this can greatly improve the design and study efficiency of a WDPR support system in wind tunnel test, which is of great significance for the engineering application of WDPRs in wind tunnels.

In future study, WDPR-8 with different aircraft models will be installed in a low-speed wind tunnel to test the performance of the suspension system. Besides, the variable stiffness control of the WDPR will be realized based on more efficient wire tension solution. As a result, the stiffness and workspace will be expected to be improved. Possible singularity in workspace will have influence on the function of the robot which also need to be studied. These works will greatly improve the stability and accuracy of the WDPR as a suspension system in wind tunnel test.

Author contribution. Qi Lin conceived and designed the study. Miaoqiao Peng designed the experiments and conducted data gathering. Yangfeng Ji performed statistical analyses and wrote the article.

Financial support. The research was facilitated by grants from the National Natural Science Foundation of China (N^o11472234 and N^o11072207), the Natural Science Foundation of Fujian Province (N^o2021J05164), and the Scientific Research Foundations of Jimei University, Chengyi College (JMT00117).

Competing interests. The author(s) declare none.

Ethical standards. The authors assert that all procedures contributing to this work comply with the ethical standards of the relevant national and institutional committees on human experimentation and with the Helsinki Declaration of 1975, as revised in 2008. The authors assert that all procedures contributing to this work comply with the ethical standards of the relevant national and institutional guides on the care and use of laboratory animals.

References

- [1] M. H. Tuttle and B. B. Gloss, *Support Interference of Wind Tunnel Models: A Selective Annotated Bibliography* (NASA Langley Research Center, Hampton, VA, USA, 1981).
- [2] T. Lambert, B. Vukasinovic and A. Glezer, "A six degrees of freedom dynamic wire-driven traverse," *Aerospace* **3**(2), 11 (2016).
- [3] P.A. Martin and P. S. Suarez, "Carton.A novel design for fully constrained planar cable-driven parallel robots to increase their wrench-feasible workspace," *Mech Mach Theory* **180**, 105159 (2023).
- [4] A. Berti, J. P. Merlet and M. Carricato, "Solving the direct geometrico-static problem of underconstrained cable-driven parallel robots by interval analysis," *Int J Rob Res* **35**(6), 723–739 (2016).
- [5] X. Tang and Z. Shao, "Trajectory generation and tracking control of a multi-level hybrid support manipulator in FAST," *Mechatronics* **23**(8), 1113–1122 (2013).
- [6] E. D. Flores-Salazar, E. Lugo-González, M. Arias-Montiel and J. Gallardo-Alvarado, "A robust control scheme for a 2PUS+RR parallel robot for ankle rehabilitation," *Robotica* **41**(11), 3296–3313 (2023). doi: [10.1017/S0263574723000978](https://doi.org/10.1017/S0263574723000978).
- [7] A. Ahmadi N, A. Kamali Eigoli and A. Taghvaeipour, "Adaptive backstepping controller based on a novel framework for dynamic solution of an ankle rehabilitation spherical parallel robot," *Robotica* **42**(5), 1568–1596 (2024).
- [8] J.-H. Duan, Z.-F. Shao, H. Liu, Z. Zang, Y. Wang and H. Zhao, "Design Analysis of a Cable-Driven Parallel Robot with Parallel Cables for Ship Side Painting," **In: Proceedings - 2023 8th International Conference on Automation, Control and Robotics Engineering, CACRE, (2023)** pp. 209–215.
- [9] M. John, C. Paolo, M. Joseph, B. Riley, D. Charles and J. Edward, "Demonstration of a Wire Suspension System for Dynamic Wind Tunnel Testing," **In: 42nd AIAA Aerospace Sciences Meeting and Exhibit, Aerospace Sciences Meetings, (2004)** pp. 10478–10487.
- [10] X.-G. Wang, S.-Y. Ma and Q. Lin, "Hybrid Pose/Tension Control Based on Stiffness Optimization of Cable-Driven Parallel Mechanism in Wind Tunnel Test," **In: Proceedings - 2016 the 2nd International Conference on Control, Automation and Robotics, ICCAR, (2016)** pp. 75–79.
- [11] X.-G. Wang, M.-J. Peng, Z.-H. Hu, Y. Chen and Q. Lin, "Feasibility Investigation of Large-Scale Model Suspended by Cable-Driven Parallel Robot in Hypersonic Wind Tunnel Test," **In: Proceedings of the Institution of Mechanical Engineers, Part G: Journal of Aerospace Engineering, (2017)** pp. 2375–2383.
- [12] Y.-Q. Wang, Q. Lin, Z. Lei, X. Shi and L. Wang, "Backstepping sliding mode robust control for a wire-driven parallel robot based on a nonlinear disturbance observer," *Math Prob Eng* **2020**(6), 3146762:P1–P17 (2020).
- [13] X.-G. Wang, Q. Lin and M. J. Peng, "Workspace analysis and verification of cable-driven parallel mechanism for wind tunnel test," *Proc Inst Mech Eng Part G: J Aerosp Eng* **231**(6), 1012–1021 (2017).
- [14] Q.-L. Chen, Q. Lin, G.-W. Wei and L. Ren, "Tension vector and structure matrix associated force sensitivity of a 6-DOF cable-driven parallel robot," *Proceedings of the Institution of Mechanical Engineers, Part C: Journal of Mechanical Engineering Science* **236**(1), 100–114 (2022).
- [15] Y.-P. Keum, H.-S. Yeol and H. Jae, "Development of a cable suspension and balance system and its novel calibration methods for effective wind tunnel tests," *Meas: J Int Meas Confed* **170**(1), 108717: P1–P14(2021).
- [16] N. Alemdaroglu, I. Iyigun, M. Altun, H. Uysal, F. Quagliotti and G. Guglieri, "Determination of Dynamic Stability Derivatives using Forced Oscillation Technique," **In: 40th AIAA Aerospace Sciences Meeting & Exhibit, Aerospace Sciences Meetings, (2002)**. doi: [10.2514/6.2002-528\(2002\)](https://doi.org/10.2514/6.2002-528(2002)).
- [17] M.-J. Peng, L.-H. Xiao, Q.-L. Chen, G.-W. Wei, Q. Lin and J.-Y. Zhuo, "Dynamic modeling and characterization of compliant cable-driven parallel robots containing flexible cables," *Robotica* **41**(10), 3160–3174 (2023).
- [18] I. Gursul, "Review of unsteady vortex flows over slender delta wings," *Journal of Aircraft*, 2005, **42**(2), 299–299. doi: [10.2514/1.5269](https://doi.org/10.2514/1.5269).
- [19] P. Lafourcade and M. Llibre, "First Steps Toward a Sketch Based Design Methodology for Wire-driven Manipulators," **In: IEEE/ASME International Conference on Advanced Intelligent Mechatronics, (2003)** pp. 20–24.
- [20] D. Farcy, M. Llibre, P. Carton and C. Lambert, "SASCO Wire-driven Parallel Set-up for Dynamic Tests in Wind Tunnel- review of Principles and Advantages for Identification of Aerodynamic Models for Flight Mechanics," **In: 8th ONERA-DLR Aerospace Symposium, (ODAS, Göttingen, 2007)**.
- [21] Y.-W. Xiao, Q. Lin, Y.-Q. Zheng and B. Liang, "Model aerodynamic tests with a wire-driven parallel suspension system in low-speed wind tunnel," *Chinese J Aeronaut* **23**(4), 393–400 (2010).
- [22] Y.-F. Ji, M.-J. Peng, Q. Lin and C. Yin, "Wire-driven parallel robot suspension system for SDM in a low-speed wind tunnel," *Adv Mech Eng* **15**(4), 168781322311702 (2023).
- [23] S.-L. Yue, Z. Wang and Q. Lin, "Stiffness Analysis of a Wire-Driven Parallel Manipulator," **In: CSAE 2012 - Proceedings, 2012 IEEE International Conference on Computer Science and Automation Engineering**. doi: [10.1109/CSAE.2012.6272901](https://doi.org/10.1109/CSAE.2012.6272901) (2012).
- [24] J. Bolboli, M. A. Khosravi, F. Abdollahi, "Stiffness feasible workspace of cable-driven parallel robots with application to optimal design of a planar cable robot," *Robot Auton Syst* **114**, 19–28 (2019).
- [25] H. Yuan, E. Courtielle and D. Deblaise, "Static and dynamic stiffness analyses of cable-driven parallel robots with non-negligible cable mass and elasticity," *Mech Mach Theory* **85**, 64–81 (2015).
- [26] H. Xiong and X. Diao, "The Effect of Cable Tensions on the Stiffness of Cable-Driven Parallel Manipulators," **In: IEEE International Conference on Advanced Intelligent Mechatronics, (2017)** pp. 1185–1190.
- [27] H. Xiong and X. Diao, "The effects of cables' strain and specific stiffness on the stiffness of cable-driven parallel manipulators," *Proc Inst Mech Eng Part C* **233**(15), 5448–5459 (2019).

- [28] V. Ferravante, E. Riva, M. Taghavi, F. Braghin and T. Bock, “Dynamic analysis of high precision construction cable-driven parallel robots,” *Mech Mach Theory* **135**, 54–64 (2019).
- [29] M. R. Mousavi, M. Ghanbari, S. A. A. Moosavian and P. Zarafshan, “Rapid and safe wire tension distribution scheme for redundant cable-driven parallel manipulators,” *Robotica*. **40**(7), 2395–2408 (2022). doi: [10.1017/S0263574721001703](https://doi.org/10.1017/S0263574721001703).
- [30] J.-S. Yu, J.-G. Tao, G. Wang, X. Li and H. Wang, “Stability analysis and optimal design of a cable-driven parallel robot,” *Robot Auton Syst* **173** (2024). doi: [10.1016/j.robot.2023.104611](https://doi.org/10.1016/j.robot.2023.104611).
- [31] B.-L. Wen, G.-L. Yang, S. H. Yeo and S. K. Mustafa, “A Generic Force-Closure Analysis Algorithm for Cable-Driven Parallel Manipulators,” *Mech Mach Theor* **46**, 461265–461275 (2011).
- [32] X. Diao and O. Ma, “Force-closure analysis of 6-DOF cable manipulators with seven or more cables,” *Robotica* **27**(2), 209–215 (2009).
- [33] L. P. Erm, “An Experimental Investigation into the Feasibility of Measuring Static and Dynamic Aerodynamic Derivatives in the DSTO Water Tunnel,” *In: 30th AIAA Applied Aerodynamics Conference*, (2012). doi: [10.2514/6.2012-3119](https://doi.org/10.2514/6.2012-3119).
- [34] N. Alemdaroglu, I. Iyigun, M. Altun, H. Uysal, F. Quagliotti and G. Guglieri, “Determination of Dynamic Stability Derivatives using Forced Oscillation Technique,” *In: 40th AIAA Aerospace Sciences Meeting and Exhibit*, (2002). doi: [10.2514/6.2002-528](https://doi.org/10.2514/6.2002-528).